Monolithic in-plane integration of gate-modulated switchable supercapacitors (ipG⊠Cap)

Yannik Bräuniger
TU Dresden
Stefanie Lochmann
TU Dresden
Christin Gellrich
TU Dresden
Lydia Galle
TU Dresden
Julia Grothe
TU Dresden
Stefan Kaskel (stefan.kaskel@tu-dresden.de)
TU Dresden https://orcid.org/0000-0003-4572-0303

Article

Keywords: supercapacitor, iontronics, nanoporous carbon, electroadsorption, inkjet printing

Posted Date: November 23rd, 2021

DOI: https://doi.org/10.21203/rs.3.rs-1079038/v1

Monolithic in-plane integration of gate-modulated switchable supercapacitors (*ip*G-Cap)

Yannik Bräuniger[a], Stefanie Lochmann[a], Christin Gellrich[a], Lydia Galle[a], Julia Grothe[a], Stefan Kaskel[a]*

[a] Y. Bräuniger, Dr. S. Lochmann, C. Gellrich, Dr. L. Galle, Dr. J. Grothe, Prof. S. Kaskel*

Department of Inorganic Chemistry I

Dresden University of Technology

Bergstraße 66, 01069 Dresden, Germany

e-mail: stefan.kaskel@tu-dresden.de

ABSTRACT

Monolithic integration of iontronic devices is a key challenge for future miniaturization and system integration, in particular the interconnection of multiple functional elements as required for ion computing. The G-Cap, a novel iontronic element, is a switchable supercapacitor with gating characteristics comparable to transistors in electronic circuits, but switching relies on ionic currents and ion electroadsorption. We report here the first monolithic in-plane G-Cap integration through 3D-inkjet printing of non-toxic nanoporous carbon precursors. The printed G-Cap has a three-electrode architecture integrating a symmetric "working" micro-supercapacitor (W-Cap) and a third "gate" electrode (G-electrode) that reversibly depletes/injects electrolyte ions into the system, effectively controlling the "working" capacitance. The printed precursor structures were directly converted into nanoporous carbon materials with a specific surface area of 544 $m^2\ g^{-1}$. The symmetric W-Cap operates with a proton conducting hydrogel electrolyte based on PVA/H_2SO_4 and shows a high capacitance (1.3 mF cm^{-2}) that can be switched “on” and “off” by applying a DC bias potential (- 1.0 V) at the G-electrode. This effectively suppresses AC electroadsorption in the nanoporous carbon electrodes of the W-Cap, resulting in a high capacitance drop from an "on" to an "off" state. Printing offers far-reaching freedom of design for varying the device structure achieving superior device performance. The new monolithic structures achieve high rate performance, reversible on-off switching with an off-value as low as 0.5 % surpassing values reported so far. Establishing technologies and device architectures for functional ionic electroadsorption devices is crucial for diverse fields ranging from microelectronics and iontronics to biointerfacing and neuromodulation.

KEYWORDS

supercapacitor, iontronics, nanoporous carbon, electroadsorption, inkjet printing

Introduction

State of the art computing architectures predominately rely on semiconductors integrated into electronic circuits. A major concern in recent years is the ever increasing energy consumption caused by the widespread of handhelds, digitalization and modern communication.[1] Biogenic nerve systems instead use a complex interplay of ionic and electric currents/potentials as well as chemically defined signalling via neurotransmitters for logic operation and memory.[2–4] Such devices are genetically optimized to operate via minimal energy consumption. In this context, recently neuromorphic architectures and iontronic devices have received tremendous attention.[5–8] Such iontronic devices are explored for future information processing as well as biointerfacing.[9–12]

Supercapacitors (electric double layer capacitors, EDLCs) are energy storage devices relying on purely physical ion adsorption in highly porous carbons.[13–16] They have been optimized over decades to achieve higher and higher energy and power density.[17,18] In particular rapid charging and discharging is an important characteristic in their commercial application for break-energy recuperation or as power boosters for electric engines in cranes[19], elevators[20] and trains.[21,22]

Developing supercapacitors (EDLCs) as active functional elements represents a change in paradigm. The integration of more complex functionality, in particular switchability, may pave the way towards advanced ion-based computer architectures, logic architectures or switchable devices. A first step in this direction is the ion-based asymmetric supercapacitor diode (CAPode) enabling unidirectional energy storage via pore size engineering and an ion-sieving mechanism effectively blocking the negative bias charging direction.[8] More recently we presented the first switchable EDLC architecture with gating characteristics (G-Cap) resembling a transistor architecture based on ion electroadsorption (Figure 1).[23] The structure consists of a simplified symmetric carbon electrode design as an AC-driven supercapacitor (working supercapacitor, W-Cap) controlled by a third porous carbon gate electrode (G-electrode; Figure 1a) arranged in a co-planar sandwich assembly. The charge storage capacity of the W-Cap is controlled by stimulated cation adsorption in the gate electrode, effectively depleting the electrolyte concentration. By applying a positive or negative bias potential on the G-electrode, the W-Cap can be effectively switched “on” or “off” (Figure 1c).[23]

Switching elements such as the G-Cap are the basis of logic families to establish transistor-transistor or diode-transistor logic gates (AND, OR, NAND, NOR).[6,24–26]

However, a key requirement for assembling active iontronic elements such as CAPode and G-Cap into more complex circuits, e.g. networks of iontronic elements, is an in-plane realization suitable for in-plane interconnection into iontronic circuits and the respective technologies for manufacturing. The original assembly of the gate electrode by sandwiching (Figure 1a) is inappropriate for such a development. A conceptual design of an in-plane G-Cap architecture is required without reducing the ion-depletion capability of the gate. The interplay of conceptual design and rapid prototyping is essential to achieve a high on-off ratio and rapid switching characteristics. Additive manufacturing technologies such as inkjet printing provide such a high degree of freedom in terms of architecture design.[27–29]

In the following, we demonstrate the realization of highly effective in-plane G-Cap architectures (*ip*G-Cap) by direct printing of a liquid carbon precursor using a nanopiezoelectric pipet on a 3D-printer. The resulting active material is a nanoporous additive-free carbon with high specific surface area.

By tailoring the characteristic dimensions of the gate and collector electrodes we achieve ideal balancing for a high on-off ratio. A hierarchical ion-transport channel arrangement is demonstrated to be essential for a rapid switching process.

The newly developed in-plane switchable supercapacitors may not-only pave the way towards ion-based computing architectures. They are also valuable devices for selectively analysing electroadsorption kinetics of electrolyte ions, complex biomolecules or even neurotransmitters and may be applicable for drug delivery and neuromodulation in future.[30–32]

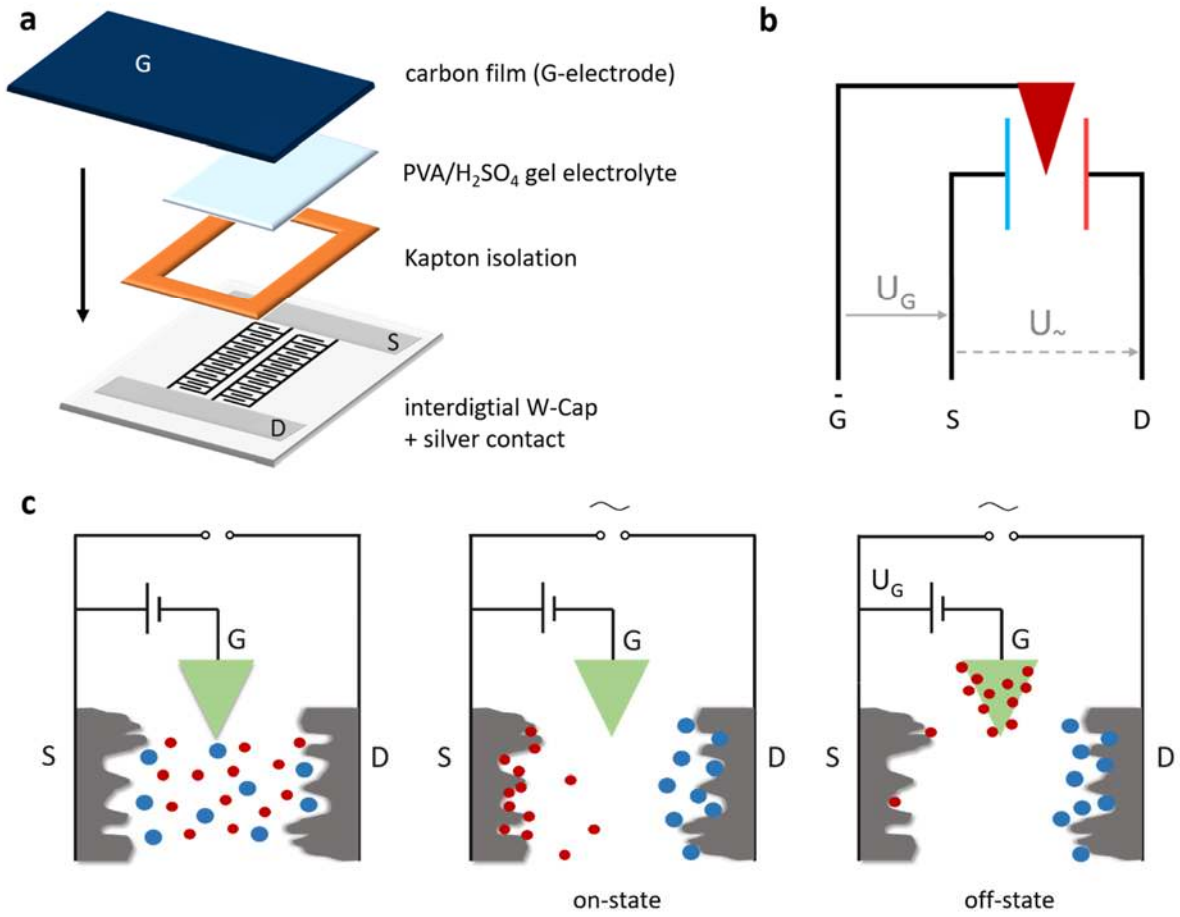

Figure 1. Function and architecture of the G-Cap.[23]

a Sandwich design. **b** Electric circuit diagram. **c** Schematic illustration of the electroadsorption-based switching process (s = source, d = drain).

Results and Discussion

In the following, we develop a novel in-plane design for planar G-Cap devices. Within this development process three generations of architectures were explored and compared (Figure 2a-d). All architectures are based on the three-electrode structure of a G-Cap in which the gate electrode enframes the two working electrodes of the W-Cap. The different G-Cap generations operate with capacitance ratios W/G ranging from 0.04 to 0.07 and electrolyte/carbon ratio comparable to the original sandwich design.[23]

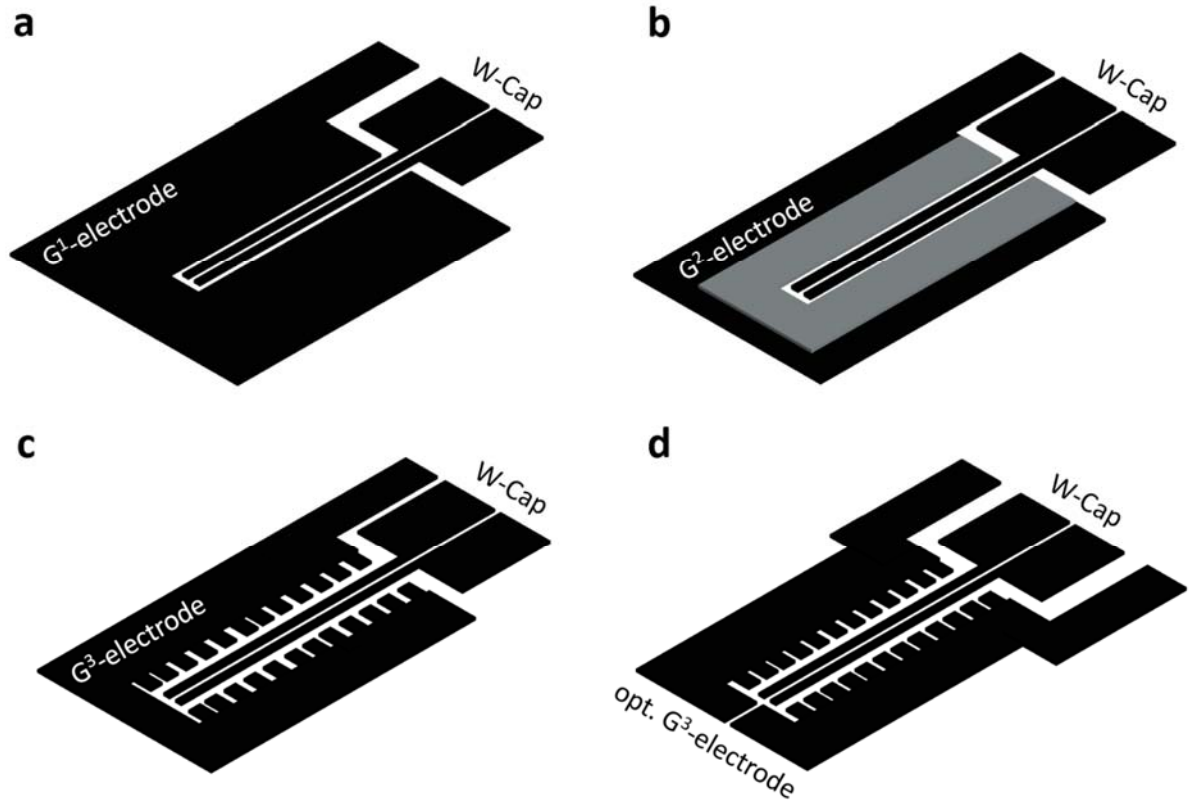

Figure 2. Architectures for in-plane G-Cap devices.

a 1st Generation with an overbalanced G-electrode. **b** 2nd Generation with enhanced G-electrode volume (gray, additional inner electrode layer). **c** 3rd Generation with a hierarchically structured G-electrode. **d** 3rd Generation with a hierarchically structured and divided G-electrode.

1st generation G-Cap architecture (ipG1-Cap)

For development of the first generation using piezoelectric printing, we printed a large area of nanoporous G-electrode as required for overbalancing. The latter is essential for effective depletion of ions to modulate the W-Cap capacitance. The W-Cap and the gate electrode were printed simultaneously and the electrolyte channel was minimized in dimensions (Figure 2a) (Supplementary Figure 1a-b).

Before measuring the switching behaviour, we evaluate the performance of the G-electrodes and the W-Cap in the symmetrical two-electrode setup using a proton-conducting PVA/H_2SO_4-based hydrogel electrolyte. Device wetting is essential to achieve rapid switching and high on-off ratios. This wetting

process is realised with several cycles of adsorption with a negative bias of - 1.2 V and desorption of ions with a reversal of the potential to + 1.0 V. We expect an excess of specific capacitance of the gate electrode to be necessary in order to obtain a good switching behaviour. Cyclic voltammograms (CVs) of the simplified interdigitated W-Cap show the typical rectangular shape for different scan rates and a capacitance of 0.2 mF (5 mV s^{-1}) is achieved (Table 1a). To measure the electrochemical capacitance, the gate electrode was split symmetrically (Supplementary Figure 2a). For the area-enhanced G-electrode, high currents and a capacitance of 5.3 mF (5 mV s^{-1}) are achieved. The ESR (equivalent series resistance) value taken from the Nyquist plot is around 830 Ω for the W-Cap (Supplementary Figure 3 and 4, Supplementary Table 1).

When a negative bias voltage is applied at the G-electrode during W-Cap operation, polarisation occurs, cations in the electrolyte are depleted and the W-cap capacitance decreases due to a deficit of charge carriers. Thus, these ions are no longer accessible for the formation of an electrical double layer and the W-Cap is switched "off" (Figure 1c). To return to an on-state, the reversed process i.e. ion desorption is forced by applying a positive bias at the G-electrode. Cations are injected back into the hydrogel electrolyte and capacitance ideally recovers to 100 % (Supplementary Figure 5).

The switching sequence for the 1st generation in-plane G-Cap (*ip*G^{1}-Cap) is shown in a capacitance retention profile (Figure 3a). W-Cap is continuously cycled at a scan rate of 50 mV s^{-1} between 0 and 0.5 V with a capacitance of 100 % before G-switching. After polarising the gate electrode to - 1.0 V, the W-Cap capacitance initially increases and then decreases very slowly down to a residual capacitance of 49 %. This result demonstrates effective proof-of-concept but the on-off ratio is inacceptable presumably due to high diffusion limitations. The first cycles even show an increase in the capacitance retention possibly through an increase in the potential difference. Due to the large area of the gate, ions must diffuse long distances to adsorb on the entire inner surface of the G-electrode which limits the electrode utilization. The ion diffusion process effectively takes place in the printed G-electrode (thickness = 220 nm) and the area above (electrolyte gel thickness above = 1 µm). In addition, the G-electrode remains polarised after disconnecting. Complete desorption of the protons from the nanoporous G-electrode and switching back is realised by applying a positive bias potential of + 1.0 V. This forces protons back into the gel electrolyte and the W-Cap capacitance returns nearly

to the initial "on" value of 100 % after some cycles. The corresponding CV-curves of different states are shown (Figure 3b). In the cyclic measurement with a scan rate of 50 mV s^{-1}, the interdigitated W-Cap has a narrow CV-shape with no redox reactions. The CV signal in off-state clearly demonstrates the reduced capacitance and the principle of switching properties in a G-Cap device. After desorption, CV-curves of the W-Cap are similar to the initial curve, proving reversible on/off switching. However, since the capacitance on-off ratio in this *ip*G^1-Cap is not sufficient (only 51 % capacitance reduction), the focus for geometry optimisation has to address diffusion limitations to achieve lower W-capacitance in the off-state. These diffusion limitations are also evident after analysing the rate capability of the G-electrode. The capacitance values decrease significantly by increasing the scan rate (Table 1a).

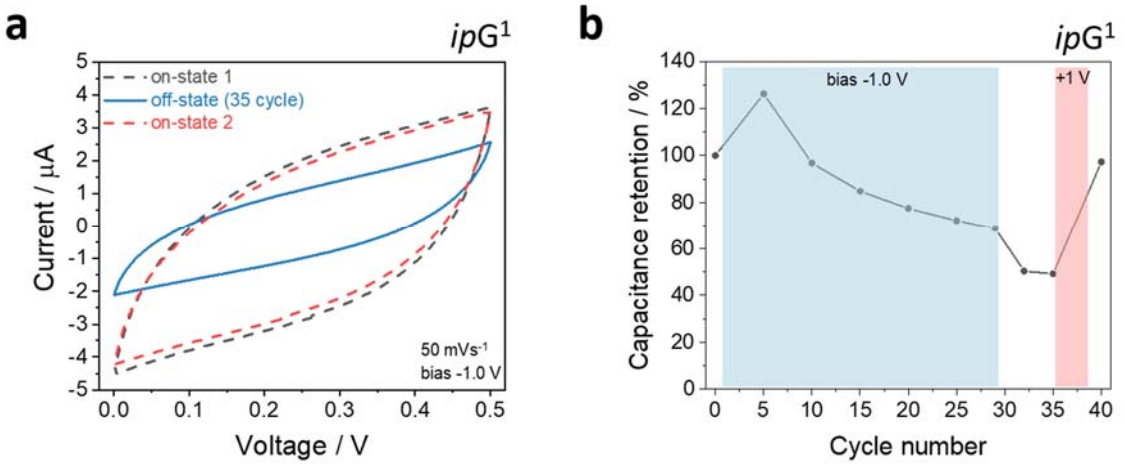

Figure 3. Representative switching behaviour measurements for the 1st generation of *ip*G-Caps. **a** CV-curves in the on- and off-state using a scan rate of 50 mVs^{-1}. **b** W-capacitance evolution during switching.

2nd Generation with reduced gate electrode footprint (ipG2-Cap)

In order to enhance the utilization of the G-electrode we designed the second generation (*ip*G^2-Cap) by reducing the gate area and increasing the height leading also to a slightly higher electrode volume (Figure 2b) (Supplementary Figure 1c).

For the new gate electrode geometry, cyclic voltammetry measurements were performed in the same setup as for *ip*G^1-Cap (Supplementary Figure 2b). Compared to *ip*G^1, the capacitance of the G^2-electrode is similar at 5.2 mF (5 mV s^{-1}) (Table 1b). The resistance of this optimised setup shows higher values than the area-expanded gate electrode (Supplementary Figure 6).

The characterisation of the switching behaviour for the second geometry is shown in a capacitance retention profile (Figure 4a). Switching measurement is performed under the same settings as illustrated for *ip*G^1-Cap and after the same wetting process at - 1.2 V. After polarising the bias electrode to - 1.0 V, the W-Cap capacitance slowly decreases. Thereby, capacitance remains similar during the first five cycles indicating significant adsorption limitations of cations. Obviously, protons are kinetically hindered to effectively electroadsorb inside this higher carbon G^2-electrode. This diffusion hindrance is a consequence of the higher thickness of the printed G-electrode (thickness = 540 nm). However, a significantly improved off-capacitance of only 20 % for the W-Cap can be achieved (Figure 4b). Thus, the G-electrode optimisation results in a significantly lower residual capacitance and a factor of two in efficiency improvement. However, after several measurements, a high loss of capacitance of the W-Cap is evident in the “on-state”, since ions do not completely desorb from the G^2-electrode during the short reversal of the potential. Due to high diffusion limitations for electroadsorption of cations, switching measurements were performed at a lower scan rate (20 mVs^{-1}) (Figure 4c). Under these conditions an efficient electroadsorption was observed at the G^2-electrode resulting in a W-capacitance reduction down to 15 % (Figure 4d).

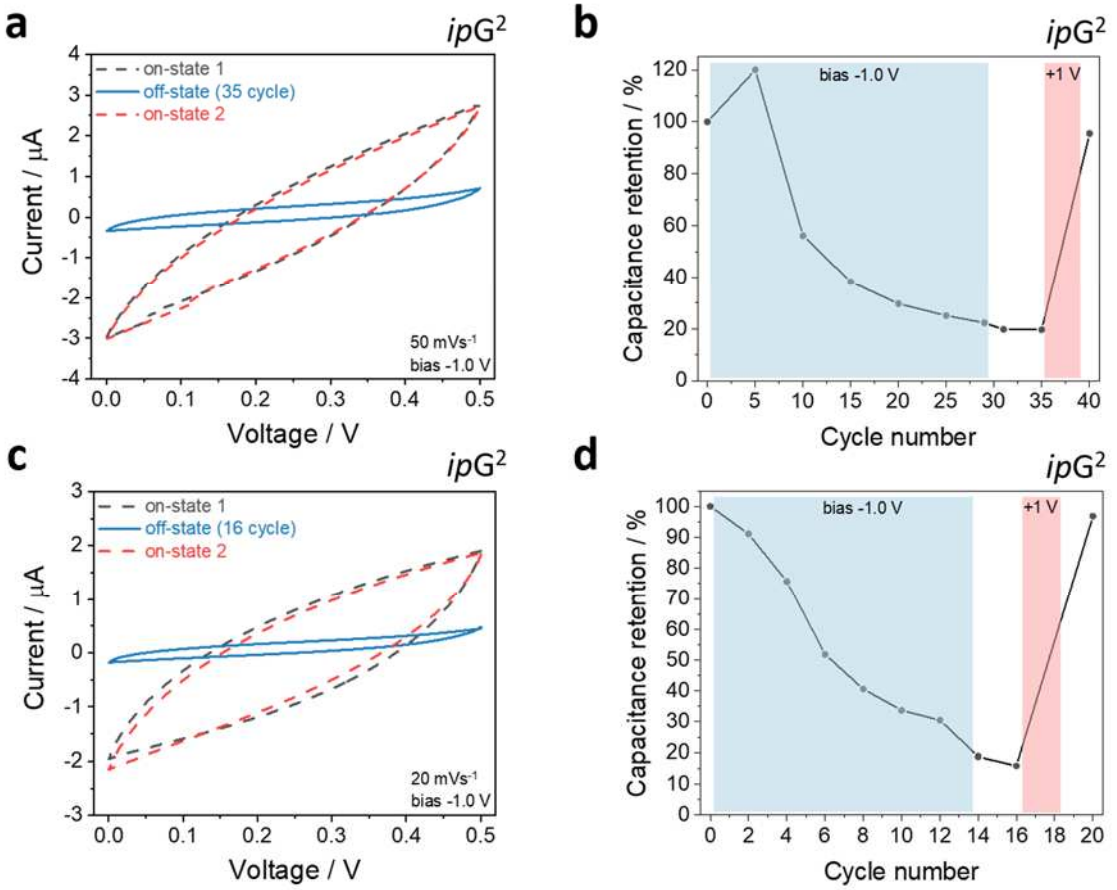

Figure 4. Representative switching behaviour measurements for the 2nd generation of *ip*G-Caps. **a** CV-curves in the on- and off-state (scan rate: 50 mVs^{-1}) 20 mVs^{-1}. **b** Capacitance retention evolution (scan rate: 50 mVs^{-1}). **c** CV-curves in the on- and off-state (scan rate: 20 mVs^{-1}). **d** Capacitance retention evolution (scan rate: 20 mVs^{-1}).

3rd Generation ipG³-Cap with hierarchical gate electrode for enhanced ion transport

In the foregoing generations a crucial limitation was the rate of electroadsorption in the G-electrode. A further adjustment of the G-electrode geometry considers hierarchical channels to reduce adsorption rate limitations and prevent resulting capacitance loss of the device. For this purpose, the total G-electrode volume is increased by printing several layers. In addition, structuring of the electrode is performed to introduce wider transport channels and increase the external surface area and ion transport (Figure 2c). The electrode is structured by small electrode fingers with a width of 550 µm and short distances of 100 µm separating each finger (Supplementary Figure 1c, d).

In cyclic voltammetry measurements, small changes in capacitance are observed as a result from patterning of the G-electrode. Compared to the *ip*G^2-Cap geometry, the capacitance of the G^3-electrode is lower at 3.0 mF (5 mV s^{-1}) (Table 1c). The electrical resistance of the G^3-electrode is very similar to the G^1-electrode. Compared to previous G-electrodes, the CV curves are rectangular as desired for a typical supercap (Supplementary Figure 7).

The capacitance switching profile for *ip*G^3-Cap shows excellent performance and the switching behaviour (Figure 5a). Before measurement, a wetting process at a negative bias - 1.2 V was applied for this architecture. The *ip*G^3-Cap switches off rapidly after the bias electrode is polarised to - 1.0 V, in particular as compared to the other geometries. We attribute this rate increase to the hierarchical pattern of the gate G^3. Thus, the rate of the ion adsorption and utilization of the gate could be increased clearly. Moreover, a very low off-capacitance of only 1.8 % can be achieved in *ip*G^3-Cap (Figure 5b). Electrode patterning shows a great positive effect in manipulating the W-Cap capacitance. The electrode fingers of the G^3-electrode act as ion channels for rapid transport and better accessibility of the electroadsorbing gate electrode. The better properties of the structured *ip*G^3-Cap are illustrated by the higher reduction of the capacitance in shorter cycle values, because cations could pass quickly and easily through the ion channels to the G^3-electrode. However, we observed reproducibility limitations and suspected insufficient electrowetting of all electrodes as a limiting factor.

Hence, for improving the reproducibility, the G-electrode was partitioned into two separate electrodes, (Figure 2d) in order to perform an independent electrowetting process by cycling the two parts of G^3-electrodes against each other. With improvement of the wetting process, the capacitance switching behaviour should become more consistent and reproducible.

After dividing the G^3-electrode, an electrowetting process at a lower negative bias voltage of -1.0 V could be used. Subsequently, the switching behaviour was characterised as described above (Figure 5c). The positive effect of the patterned electrodes is demonstrated by a better accessibility of the ion adsorption. Due to the improved wetting process, a suppression of residual W-capacitance down to 0.5 % can be achieved (Figure 5d). Thus, the structure adaptation and the lower bias potential results in an increase of reproducibility of a fast switching characteristic and a high on-off ratio.

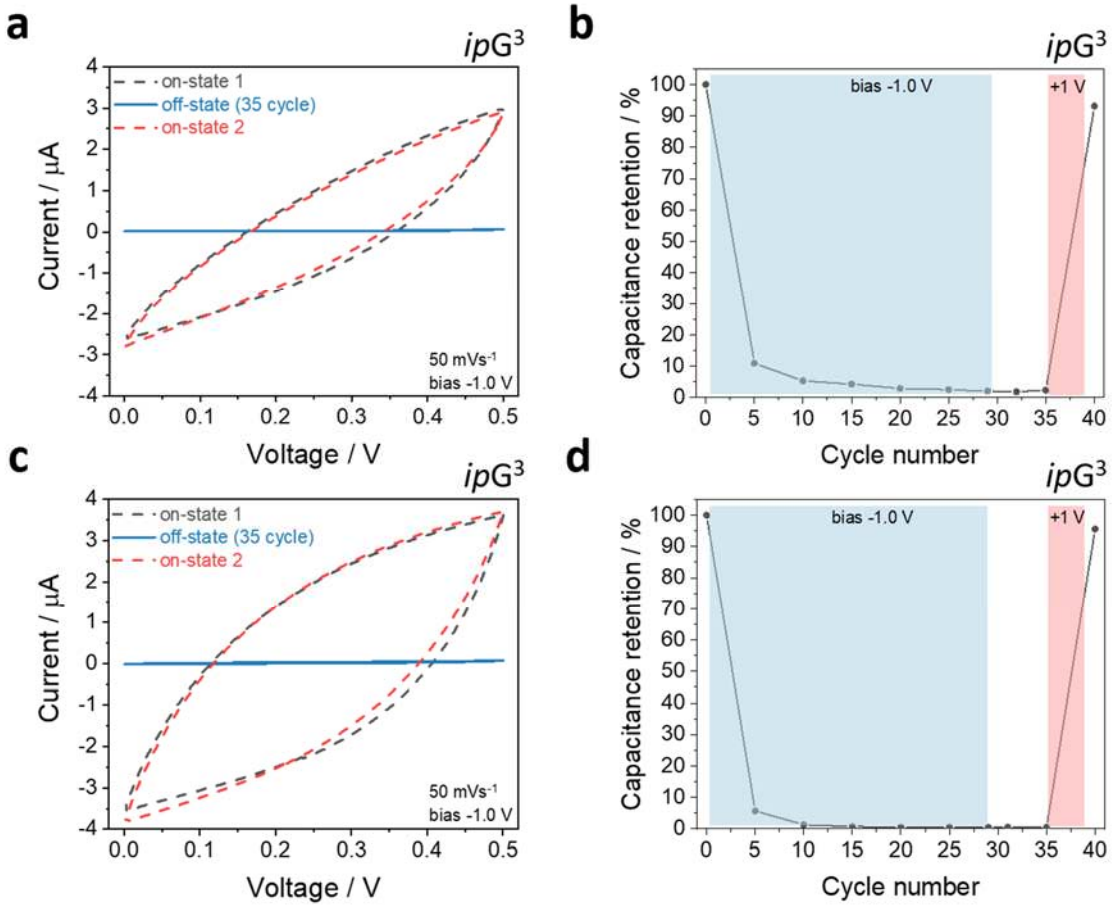

Figure 5. Representative switching behaviour measurements for the 3rd generation of *ip*G-Caps. **a** CV-curves in the on- and off-state at a scan rate of 50 mVs^{-1} for the hierarchical G^3-electrode. **b** Capacitance retention evolution for the hierarchical G^3-electrode. **c** CV-curves for the divided hierarchical G-electrode. **d** Capacitance retention evolution for the divided hierarchical G-electrode.

By optimizing G-electrode architectures for in-plane G-Cap devices in the different generations, the switching behaviour was significantly improved and diffusion limitations were eliminated.

For a quantitative analysis of the switching rate we evaluated the time ($\tau_{1/2}$) needed to reduce the W-capacitance to 50 % of the initial value. While the *ip*G^1 is slow ($\tau_{1/2}$ = 658 s) the optimized *ip*G^3 switches rapidly ($\tau_{1/2}$ = 23.3 s) (Figure 6, Table 2).

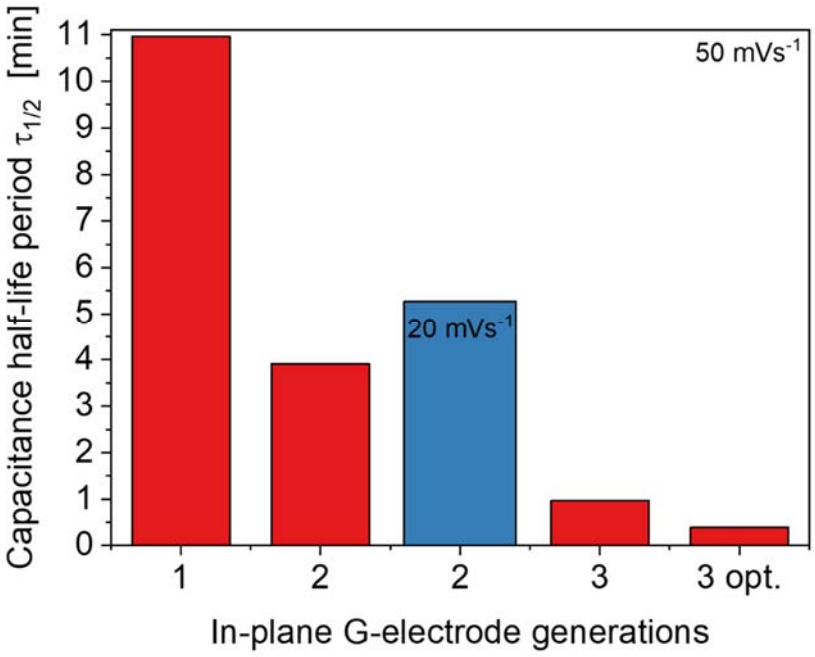

Figure 6. Switching kinetics comparing $\tau_{1/2}$ for different scan rates (20 and 50 mVs^{-1}) and G-electrode generations for planar G-Cap devices.

Conclusion

A novel switchable supercapacitor architecture (*ip*G-Cap) was produced by 3D-piezoelectric inkjet printing as a planar device. The essential elements are three nanoporous high surface area carbon electrodes obtained from a non-toxic liquid carbon precursor. An in-plane nanoporous gate electrode effectively controls the capacitance of a working capacitor (W-Cap) by regulating the ion concentration of a gel electrolyte. Rapid prototyping of various gate electrode geometries gives insight into ion adsorption mechanisms, rate-determining transport and adsorption phenomena in the electroadsorption device to optimise the capacitance switching characteristics by electrolyte depletion between on- and off-states, in particular rate and on/off ratio. The target of structural design was to achieve reversible switching with the highest possible on-off-ratio and a high capacitance regeneration. With the lowest off-value of 0.5 % residual capacitance the *ip*G^3-Cap even outperforms earlier reports.[23] Due to purely physical ion adsorption of supercapacitors, a fast and repetitive switching behaviour without degeneration is enabled. In particular, pore accessibility at reduced

diffusion limitations of ions appeared to be important for the in-plane G-Cap mechanism. Our work is a key step towards interconnecting discrete iontronic elements such as G-Caps and CAPodes into more complex iontronic circuits. Despite the switching rates are not comparable with those of electronic transistors further miniaturization is expected to enable higher frequency operation. We envision multiple G-Caps interconnected in-plane in architectures for realizing logic gates. Such logic gates could be used for the power management of autonomous microelectronic devices or even lead to more complex ion-computing architectures. For in-plane printing CAPodes it will be necessary to also print nanoporous carbons with narrow pore size distribution, which can lead to selective ion screening for precise adjustment of the pore size.[8] Further work is necessary to access also a wider voltage window using organic electrolytes.[33] Beyond iontronics, printed G-Cap essays may offer new opportunities in fundamental research for the investigation of ion diffusion and electroadsorption mechanisms through selective analysis of adsorption kinetics. Developing new functional electroadsorption devices and architectures is an essential step towards their implementation in ion transistor circuits, biointerfacing or neuromodulation in future.

Methods

Carbon precursors

The sucrose precursor was obtained by mixing 1.5 g (4.38 mmol) sucrose (> 99 %, *AppliChem*) in 8.64 mL de-ionised water and 0.15 g (1.53 mmol) concentrated sulphuric acid (95 %, *VWR*). The solution was treated by ultra-sonication for 20 minutes. Subsequently, 1.76 mL (29.8 mmol) ethanol (99.98 %, *VWR*) was added dropwise to the clear and homogenous solution under stirring.

Electrolyte

For the synthesis of the solid-state electrolyte PVA/H_2SO_4 0.5 g (11.35 mmol) polyvinyl alcohol (PVA; ≥ 98 %, *Merck*; molecular weight 145,000 g mol^{-1}) was dissolved in 7 ml de-ionised water and stirred at 85 °C. 0.5 g (5.10 mmol) sulphuric acid (95 %, *VWR*) was added to the solution under vigorous stirring for 1 h. The clear electrolyte was used for the preparation of G-Caps.

Piezoelectric inkjet printing

The piezo-printing for the preparation of G-Cap structures was realised using a *BioScaffolder 3.2* and a piezoelectric micropipetting tip *Nano-Tip J* from *GeSiM mbH*. The pipetting tip has a drop volume of approx. 400 pL, a chamber volume of 0.7 µL and a maximal operating frequency of 1,000 Hz. The parameters (frequency, pulse width, voltage) were adjusted to form drops at the piezoelectric micropipetting tip (150 Hz, 90 µs, 55 V). The adjustments were made using a stroboscopic camera. Glass substrates (*Corning® 1737*, *DELTA Technologies substrates*) (25 mm × 25 mm × 1.1 mm) were used for printing the carbon precursors. They were pre-treated in a piranha solution (1 part 30 % H_2O_2, *Fisher Chemicals*; 3 parts conc. H_2SO_4) for 20 minutes. After cleaning them with de-ionised water and ethanol, they were dried in a nitrogen steam. The glass substrates were heated to a temperature of approx. 80 °C on a heating plate. An interdigital structure was printed on the hot glass substrate with precursors using defined printing parameters[27]. After printing, the dimensions were analysed using a light microscope from *Breukhoven Microscope Systems BMS*.

The precursor was absorbed through the tip by vacuum and subsequently electrical voltage causes the formation of precursor droplets at the tip. The voltage is modulated by a pulse width and a certain frequency. As a result, drops are formed at the tip in the micron-size range (200 µm). The pyrolysis of the printed structures was carried out at 900 °C for 2 h under argon with a constant heating rate of 150 K h^{-1}.

Preparation of G-Cap structure

The pyrolysed G-Cap electrodes were contacted with silver conducting paste (*Ferro GmbH*) on the contact pads. Furthermore, an area of 6 × 9 mm around the electrode was sealed with Kapton® foil to define the reservoir for the gel electrolyte. Hereafter, the electrode was activated with cold-inductive coupled argon plasma, which was generated with a plasma finger *KINPEN* (*Neoplas Tools*) and 10 µL PVA/H_2SO_4 hydrogel electrolyte was deposited on top. After drying at room temperature, the electrochemical characterisation was carried out.

Electrochemical characterisation

Symmetric interdigital supercapacitors were analysed with a *VMP3* potentiostat from *BioLogic Science Instruments* in a two electrode setup. Cyclic voltammetry was measured with scan rates of 5 and 100 mV s^{-1} in a potential range of 0 to 1.0 V. The capacitances of the simplified interdigitated W-Cap and G-electrode architectures in three generations were normalized to the device area (Supplementary Figure 8, Supplementary Table 1-3).

The G-Cap was analysed in a CE to ground setup synchronising two ports with a combined working electrode. Cyclic voltammetry during the switching process between W-Cap and G-Cap was carried out in a voltage range between 0 to 0.5 V and a bias of – 1.0 to 1.0 V was applied using chronoamperometry.

Author Information

Corresponding Author

Prof. Dr. Stefan Kaskel - Faculty of chemistry and food chemistry, Department of Inorganic Chemistry I, Dresden University of Technology, 01069 Dresden, Germany, e-mail: stefan.kaskel@tu-dresden.de

Authors

Yannik Bräuniger - Faculty of chemistry and food chemistry, Department of Inorganic Chemistry I, Dresden University of Technology, 01069 Dresden, Germany, e-mail: yannik.braeuniger@tu-dresden.de

Dr. Stefanie Lochmann - Faculty of chemistry and food chemistry, Department of Inorganic Chemistry I, Dresden University of Technology, 01069 Dresden, Germany, e-mail: stefanie.lochmann@outlook.de

Christin Gellrich - Faculty of chemistry and food chemistry, Department of Inorganic Chemistry I, Dresden University of Technology, 01069 Dresden, Germany, e-mail: christin.gellrich@mailbox.tu-dresden.de

Dr. Lydia Galle - Faculty of chemistry and food chemistry, Department of Inorganic Chemistry I, Dresden University of Technology, 01069 Dresden, Germany, e-mail: lydia.galle@tu-dresden.de

Dr. Julia Grothe - Faculty of chemistry and food chemistry, Department of Inorganic Chemistry I, Dresden University of Technology, 01069 Dresden, Germany, e-mail: julia.grothe@tu-dresden.de

Competing interests

The authors declare no competing financial interest.

References

1. Noussan, M., Hafner, M. & Tagliapietra, S. *The Future of Transport Between Digitalization and Decarbonization: Trends , Strategies and Effects on Energy Consumption*. (Springer Nature, 2020). doi:10.1007/978-3-030-37966-7.
2. Robin, P., Kavokine, N. & Bocquet, L. Modeling of emergent memory and voltage spiking in ionic transport through angstrom-scale slits. *Science* **373**, 687–691 (2021).
3. Tanveer, M. & Shabala, S. Neurotransmitters in Plant Signaling and Communication. in *Neurotransmitters in Signalling and Adaptation to Salinity Stress in Plants* 49–73 (Springer, 2020).
4. Yang, C. *et al.* 3D-Printed Carbon Electrodes for Neurotransmitter Detection. *Angew. Chem. Int. Ed.* **57**, 14255–14259 (2018).
5. Yang, C. & Suo, Z. Hydrogel ionotronics. *Nat. Rev. Mater.* **3**, 125–142 (2018).
6. Tybrandt, K., Forchheimer, R. & Berggren, M. Logic gates based on ion transistors. *Nat. Commun.* **3**, 871–876 (2012).
7. Bisri, S. Z., Shimizu, S., Nakano, M. & Iwasa, Y. Endeavor of Iontronics: From Fundamentals to Applications of Ion-Controlled Electronics. *Adv. Mater.* **29**, 1–48 (2017).
8. Zhang, E. *et al.* An Asymmetric Supercapacitor–Diode (CAPode) for Unidirectional Energy Storage. *Angew. Chem. Int. Ed.* **58**, 13060–13065 (2019).
9. Zhang, E., Galle, L., Lochmann, S., Grothe, J. & Kaskel, S. Nanoporous carbon architectures for iontronics: Ion-based computing, logic circuits and biointerfacing. *Chem. Eng. J.* **420**,

130431 (2021).

10. Ling, H. *et al.* Electrolyte-gated transistors for synaptic electronics, neuromorphic computing, and adaptable biointerfacing. *Appl. Phys. Rev.* **7**, 011307 (2020).
11. Stavrinidou, E. *et al.* Electronic plants. *Sci. Adv.* **1**, 1–8 (2015).
12. Bernacka-Wojcik, I. *et al.* Implantable Organic Electronic Ion Pump Enables ABA Hormone Delivery for Control of Stomata in an Intact Tobacco Plant. *Small* **15**, 1–9 (2019).
13. Wang, Y., Song, Y. & Xia, Y. Electrochemical capacitors: Mechanism, materials, systems, characterization and applications. *Chem. Soc. Rev.* **45**, 5925–5950 (2016).
14. Béguin, F., Presser, V., Balducci, A. & Frackowiak, E. Carbons and electrolytes for advanced supercapacitors. *Adv. Mater.* **26**, 2219–2251 (2014).
15. Zhao, L. *et al.* Nitrogen-containing hydrothermal carbons with superior performance in supercapacitors. *Adv. Mater.* **22**, 5202–5206 (2010).
16. Simon, P., Gogotsi, Y. & Dunn, B. Where Do Batteries End and Supercapacitors Begin? *Science* **343**, 1210–1211 (2014).
17. Simon, P. & Gogotsi, Y. Perspectives for electrochemical capacitors and related devices. *Nat. Mater.* **19**, 1151–1163 (2020).
18. Borchardt, L., Oschatz, M. & Kaskel, S. Tailoring porosity in carbon materials for supercapacitor applications. *Mater. Horizons* **1**, 157–168 (2014).
19. Kermani, M., Parise, G., Chavdarian, B. & Martirano, L. Ultracapacitors for port crane applications: Sizing and techno-economic analysis. *Energies* **13**, 1–19 (2020).
20. Jabbour, N. & Mademlis, C. Supercapacitor-based energy recovery system with improved power control and energy management for elevator applications. *IEEE Trans. Power Electron.* **32**, 9389–9399 (2017).
21. Fallah, M., Asadi, M., Moghbeli, H. & Dehnavi, G. R. Energy management and control system of DC-DC converter with super-capacitor and battery for recovering of train kinetic energy. *J. Renew. Sustain. Energy* **10**, 1–12 (2018).
22. Zhang, X. *et al.* Recent advances in porous graphene materials for supercapacitor applications. *RSC Adv.* **4**, 45862–45884 (2014).

23. Lochmann, S. *et al.* Switchable Supercapacitors with Transistor-Like Gating Characteristics (G-Cap). *Adv. Funct. Mater.* **30**, 1910439 (2020).

24. Resta, G. V. *et al.* Doping-Free Complementary Logic Gates Enabled by Two-Dimensional Polarity-Controllable Transistors. *ACS Nano* **12**, 7039–7047 (2018).

25. Pillonnet, G., Fanet, H. & Houri, S. Adiabatic capacitive logic: A paradigm for low-power logic. *Proc. - IEEE Int. Symp. Circuits Syst.* 7–10 (2017).

26. Wu, P., Reis, D., Hu, X. S. & Appenzeller, J. Two-dimensional transistors with reconfigurable polarities for secure circuits. *Nat. Electron.* **4**, 45–53 (2021).

27. Brauniger, Y., Lochmann, S., Grothe, J., Hantusch, M. & Kaskel, S. Piezoelectric Inkjet Printing of Nanoporous Carbons for Micro-supercapacitor Devices. *ACS Appl. Energy Mater.* **4**, 1560–1567 (2021).

28. Li, L. *et al.* High-Performance Solid-State Supercapacitors and Microsupercapacitors Derived from Printable Graphene Inks. *Adv. Energy Mater.* **6**, 1600909 (2016).

29. Li, B. *et al.* Direct Inkjet Printing of Aqueous Inks to Flexible All-Solid-State Graphene Hybrid Micro-Supercapacitors. *ACS Appl. Mater. Interfaces* **11**, 46044–46053 (2019).

30. Kim, S., Ozalp, E. I., Darwish, M. & Weldon, J. A. Electrically gated nanoporous membranes for smart molecular flow control. *Nanoscale* **10**, 20740–20747 (2018).

31. Zhu, J. *et al.* Ion Gated Synaptic Transistors Based on 2D van der Waals Crystals with Tunable Diffusive Dynamics. *Adv. Mater.* **30**, 1800195 (2018).

32. Song, Y. *et al.* Nitrogen-Doped Carbon Nanotubes Supported by Macroporous Carbon as an Efficient Enzymatic Biosensing Platform for Glucose. *Anal. Chem.* **88**, 1371–1377 (2016).

33. Balducci, A. Electrolytes for high voltage electrochemical double layer capacitors: A perspective article. *J. Power Sources* **326**, 534–540 (2016).

Table 1. Rate-dependent capacitances of the generations of G-electrode architectures based EDLCs (*ip*G^1-, *ip*G^2- and *ip*G^3-Cap).

Scan rates	*ip*G^1-G-electrode (**a**)	*ip*G^2-G-electrode(**b**)	*ip*G^3-G-electrode (**c**)
[mV s^{-1}]	Capacitance [mF]	Capacitance [mF]	Capacitance [mF]
5	5.3	5.2	3.0
10	4.9	4.6	2.4
20	3.4	3.4	2.2
50	2.6	2.2	1.9
100	1.6	1.2	1.7

Table 2. Capacitance decay time $\tau_{1/2}$ of G-electrode generations for *ip*G-Cap devices at different scan rates (50 mVs^{-1}, *20 mVs^{-1}).

G-electrode generations	capacitance decay time $\tau_{1/2}$ [s]
*ip*G^1	657.8
*ip*G^2	234.5
*ip*G^2*	316.5
*ip*G^3	58.1
opt. *ip*G^3	23.3

Supplementary Files

This is a list of supplementary files associated with this preprint. Click to download.

- 20211114kaskelSupplInformation.pdf